Eur. Phys. J. C (2024) 84:1016
https://doi.org/10.1140/epjc/s10052-024-13380-7

THE EUROPEAN PHYSICAL JOURNAL C

Regular Article - Theoretical Physics

Impact of Q-balls formed by first-order phase transition on sterile neutrino dark matter

Jiucheng Ma[1], **Siyu Jiang**[1,a], **Xiu-Fei Li**[2,b]

[1] MOE Key Laboratory of TianQin Mission, TianQin Research Center for Gravitational Physics and School of Physics and Astronomy, Frontiers Science Center for TianQin, Gravitational Wave Research Center of CNSA, Sun Yat-sen University (Zhuhai Campus), Zhuhai 519082, China
[2] School of Physical Science and Technology, Inner Mongolia University, Hohhot 010021, China

Received: 6 June 2024 / Accepted: 16 September 2024

Abstract We explore the mechanism that can explain the production of lepton asymmetry and two types of sterile neutrino dark matter. The first type involves heavy sterile dark matter produced directly by the decay of Q-balls which are formed by first-order phase transition in the early universe; the second consists of keV sterile neutrino dark matter, produced resonantly with the aid of lepton asymmetry from Q-ball decay. Besides, gravitational waves from cosmic strings generated during the phase transition process could be detected at future interferometers.

1 Introduction

The origin and properties of dark matter (DM) are still being explored now, with sterile neutrino being one of the famous DM candidates [1]. Among the simplest extensions of the Standard Model, right-handed neutrinos account for the non-vanishing active neutrino masses through the see-saw mechanism. In the Standard Model extended by three right-handed neutrinos, the baryon asymmetry of the universe can be explained by the CP-violating decay of the two heavier sterile neutrinos, which is the so-called leptogenesis mechanism [2]. And the lightest right-handed neutrino, being the sterile DM, can be produced through active-sterile neutrino oscillation, known as the Dodelson–Widrow (DW) mechanism [3]. However, the DW mechanism has been ruled out by the Lyman-α and X-ray constraints [4]. These constraints can be evaded by modified or alternative mechanisms, like Shi–Fuller mechanism [5], singlet decay [6–9] or evaporation of primordial black holes [10].

The Shi–Fuller mechanism requires a substantial lepton asymmetry in the universe. In order to avoid conversion into baryon asymmetry by the electroweak sphaleron process, it demands that the lepton asymmetry must be generated after the electroweak phase transition. Extensive research has been conducted on mechanisms for achieving such asymmetry, including low-scale leptogenesis from right-handed neutrino oscillations [11–13], secondary leptogenesis [14,15], and L-ball decay [16]. Notably, this significant neutrino asymmetry can be experimentally probed through precision measurements of the relativistic degrees of freedom $N_{\rm eff}$ in Cosmic Microwave Background (CMB) experiments, and also has potential implications for Big Bang Nucleosynthesis (BBN) estimates.

In this work, we propose a mechanism that can explain the production of baryon asymmetry, lepton asymmetry and sterile neutrino DM. The Q-balls are produced during $U(1)_{B-L}$ symmetry breaking. After the electroweak phase transition, the Q-balls decay into the lepton asymmetry and sterile neutrino DM. The generated lepton asymmetry can also support the production of sterile neutrino DM from resonant active-sterile neutrino oscillation. Interestingly, this mechanism can produce gravitational wave (GW) signals which can be detected by future experiments. The $U(1)_{B-L}$ breaking can produce gravitational wave spectra originating from both cosmic strings and phase transition.

This paper is structured as follows: in Sect. 2, we explore the first-order phase transition (FOPT) in the $U(1)_{B-L}$ model and its associated GW signals. Section 3 briefly discusses the baryon asymmetry arising from leptogenesis within the $B-L$ model. Section 4 discusses heavy sterile DM and keV sterile neutrino DM, both produced with assistance of Q-ball decay, and their relation to lepton asymmetry. The concise conclusion is given in Sect. 5.

[a] e-mail: jiangsy36@mail2.sysu.edu.cn (corresponding author)
[b] e-mail: xiufeili@imu.edu.cn (corresponding author)

Published online: 07 October 2024

2 $B-L$ model

We introduce three right-handed neutrinos ($\nu_R^1=\nu_s, \nu_R^2, \nu_R^3$) where the first generation is the DM candidate and one scalar $S=(v_\varphi+\varphi+i\sigma)/\sqrt{2}$ that breaks the gauged $B-L$ symmetry. We also introduce a "neutrino-philic" complex scalar Φ which directly couples only to the neutrinos and the sterile neutrino ν_s. The three right-handed neutrinos, S and Φ are charged under $B-L$ symmetry with quantum number -1, 2 and 2 respectively.

$$\begin{aligned}\mathcal{L}_{B-L}=&\sum_i \bar{\nu}_R^i i\not{D}-12.5mu/\nu_R^i+D_\mu S^\dagger D^\mu S+D_\mu\Phi^\dagger D^\mu\Phi\\&-\frac{1}{4}Z'_{\mu\nu}Z'^{\mu\nu}-V(S,\Phi)-\frac{1}{2}\sum_{i,j}\left(y_R^{ij}\bar{\nu}_R^{i,c}S\nu_R^j+\text{h.c.}\right)\\&-\sum_{i,j}\left(y_D^{ij}\bar{\ell}_L^i\tilde{H}\nu_R^j+\text{h.c.}\right)+\mathcal{L}_{decay},\end{aligned}\tag{1}$$

where we adopt the classically conformal assumption for the potential $V(S,\Phi)$,

$$V(S,\Phi)=\lambda_s|S|^4+\lambda_\phi|\Phi|^4+\lambda_{\phi s}|S|^2|\Phi|^2,\tag{2}$$

and a interaction term depicting Φ decay [17,18],

$$\mathcal{L}_{\text{decay}}=-\sum_i y_\nu^i\bar{\nu}_L^{i,c}\Phi\nu_L^i-y_s\bar{\nu}_s^c\Phi\nu_s+\text{h.c.}\tag{3}$$

We assume the vacuum expectation value of Φ is zero, so the Φ does not contribute to the masses of neutrinos and sterile neutrinos. After breaking of the $B-L$ symmetry, the right-handed neutrinos acquire Majorana masses, $M_R^{ij}=\frac{y_R^{ij}}{\sqrt{2}}v_\varphi$. As a result of the type-I seesaw mechanism, the left-handed neutrino masses are given by

$$m_\nu\simeq m_D M_R^{-1}m_D\simeq\frac{|y_D|^2v_{EW}^2}{2M_R},\tag{4}$$

where m_D is the Dirac masses after the electroweak phase transition and v_{EW} is the vacuum expectation value of the Standard Model Higgs. We will set $M_R^{ij}=\text{diag}(M_R^1,M_R^2,M_R^3)$ and $M_R^1=m_{\nu_s}$ is the mass of the lightest right-handed neutrino, the sterile neutrino. When the mass of sterile neutrino DM m_{ν_s} weighs about 10 keV, for $v_\varphi\approx10^9$GeV, the Yukawa coupling has to be satisfied $y_R^1\approx10^{-14}$. It has been shown that the sterile neutrino DM does not come into thermal equilibrium if $y_R^1\ll10^{-6}$ after inflation [19,20]. In this work we discuss two possible production mechanism of sterile neutrino DM, the contributions from decay and the active-sterile neutrino oscillation.

2.1 Effective potential

The zero temperature effective potential is given by Gildener–Weinberg potential (see Appendix A)

$$V_0(\varphi)=B_1\varphi^4\left(\log\frac{\varphi}{v_\varphi}-\frac{1}{4}\right)+\frac{B_1}{4}v_\varphi^4,\tag{5}$$

where

$$B_1=\frac{3}{2\pi^2}\left(\frac{\lambda_{\phi s}^2}{96}+g_{B-L}^4-\sum_i\frac{y_{R,i}^4}{96}\right),\tag{6}$$

The potential is defined to be zero at $\varphi=v_\varphi$. Note we have neglected the contribution from φ as $\lambda_s^2\ll\lambda_{\phi s}^2, g_{B-L}^4, (y_R^i)^4$ as usual in the Coleman–Weinberg mechanism [21,22]. The Gildener–Weinberg potential provides the scalar mass of scalar φ, $M_\varphi=2\sqrt{B_1}v_\varphi$.

The one-loop thermal corrections is

$$V_{\text{th}}=\sum_{i=\text{bosons}}\frac{n_i}{2\pi^2}T^4J_B\left[\frac{m_i}{T}\right]+\sum_{i=\text{fermions}}\frac{n_i}{2\pi^2}T^4J_F\left[\frac{m_i}{T}\right],\tag{7}$$

where m_i is the field-dependent mass, n_i denotes the degree of freedom of the bosonic/fermionic particles and thermal integral functions are defined as

$$J_{B/F}(y)=\pm\int_0^\infty dx x^2\log\left(1\mp e^{-\sqrt{x^2+y^2}}\right).\tag{8}$$

In the calculation of the thermal potential, we include contributions from daisy resummations [23,24]. Two resummation techniques can be chosen: the Parwani method [23], which incorporates thermal-corrected field-dependent masses and thermal counter-terms, and the Arnold–Espinosa method [24] where the thermal corrections are solely added in the J_B function. Our analysis utilizes the Arnold–Espinosa method. The daisy contributions are expressed as

$$V_{\text{daisy}}(\varphi,T)=-\sum_i\frac{g_iT}{12\pi}\left[(m_i^2(\varphi)+\Pi_i)^{3/2}-m_i^3(\varphi)\right],\tag{9}$$

with

$$\Pi_\Phi=\frac{\lambda_{\phi s}}{24}T^2,\quad\Pi_{Z'_L}=4g_{B-L}^2T^2.\tag{10}$$

The total finite temperature effective potential is

$$V_{\text{eff}}(\varphi,T)=V_0(\varphi)+V_{\text{th}}(\varphi,T)+V_{\text{daisy}}(\varphi,T).\tag{11}$$

2.2 FOPT

The phase transition in the early Universe involves symmetry breaking, proceeding through bubble nucleation, growth, and collide. The critical temperature T_c is defined where the effective potential's minima are degenerate, $V_{\text{eff}}(v(T_c),T_c)=$

$V_{\rm eff}(0, T_c)$, with $v(T_c)$ as the true vacuum value at T_c. Nucleation starts at the nucleation temperature T_n, where the nucleation rate is given by

$$\Gamma(T) \approx T^4 \left(\frac{S_3(T)}{2\pi T}\right)^{3/2} e^{-S_3(T)/T}, \tag{12}$$

with $S_3(T)$ being the action of the $\mathcal{O}(3)$ symmetric bounce solution [25].

The nucleation temperature T_n is typically defined by

$$\Gamma\,(T_n)\, H^{-4}\,(T_n) \approx 1, \tag{13}$$

and $H(T)$ is the Hubble expansion rate,

$$H^2(T) = \frac{8\pi}{3M_{\rm pl}^2}\left(\rho_r + \Delta V_{\rm eff}(T)\right), \tag{14}$$

where $\rho_r = \pi^2 g_\star T^4/30$ represents radiation energy density with $g_\star$ being the relativistic degrees of freedom and $M_{\rm pl} = 1.22 \times 10^{19}$ GeV is the Planck mass. The potential energy difference between the false and true vacuum is defined as

$$\Delta V_{\rm eff}(T) = V_{\rm eff}(0, T) - V_{\rm eff}(v_\varphi(T), T).$$

This potential difference drives bubble expansion in the universe, reducing the volume of the false vacuum over time. The probability of finding a point in the false vacuum reads,

$$p(T) = e^{-I(T)}, \tag{15}$$

where $I(T)$ is the fraction of vacuum converted to the true vacuum,

$$I(T) = \frac{4\pi}{3}\int_T^{T_c} dT' \frac{\Gamma\left(T'\right)}{T'^4 H\left(T'\right)}\left[\int_T^{T'} d\tilde{T}\,\frac{v_w}{H(\tilde{T})}\right]^3. \tag{16}$$

The percolation temperature T_p, is defined by $I(T_p) = 0.34$ [26,27].

We use the following definition of the phase transition strength:

$$\alpha \equiv \left.\frac{\left(1 - \frac{T}{4}\frac{\partial}{\partial T}\right)\Delta V_{\rm eff}}{\rho_r}\right|_{T=T_n}, \tag{17}$$

The inverse time duration β at nucleation temperature T_n is defined as

$$\frac{\beta}{H} = T\frac{d}{dT}\left(\frac{S_3}{T}\right)\Big|_{T=T_n}. \tag{18}$$

We use `CosmoTransitions` [28] to calculate the phase transition dynamics. Four benchmark points are shown in Table 1 where we fix $g_{B-L} = 0.05$ and $y_R^2 = y_R^3 = 1.2$. y_R^1 provides the mass of sterile neutrino DM and can be negligible. We concentrate on $\alpha \lesssim 1$ since larger values of α result in an ultra-supercooling phase transition, leading to an ultra-relativistic bubble wall velocity. In this case, Q-balls can hardly form because almost all particles will penetrate into the bubbles.

Table 1 Four sets of benchmark parameters for the $B-L$ model where we fix $g_{B-L} = 0.05$ and $y_R^2 = y_R^3 = 1.2$

	$\lambda_{\phi s}$	v_φ (GeV)	$T_{\rm n}$ (GeV)	β/H	α
BP1	3.8	10^9	1.05×10^8	72.71	0.94
BP2	4	5×10^9	5.75×10^8	70.01	0.75
BP3	4	1.3×10^{10}	1.41×10^9	64.65	0.93
BP4	4.2	5×10^{10}	5.9×10^9	62.05	0.76

2.3 GW spectra

In our scenario, two sources generate GWs: firstly, the $U(1)_{B-L}$ FOPT produces GWs through bubble collision, sound waves, and turbulence within the plasma. Secondly, the cosmic strings formed subsequent to the $U(1)_{B-L}$ breaking continuously emit GWs. We will discuss these two mechanisms in detail in Appendices B and C. The GW spectra for four benchmark points are depicted in Fig. 1, alongside various expected sensitivity curves for different detectors. We have chosen the bubble wall velocity $v_w = 0.6$, and find that the peak frequencies of the GWs generated during the FOPT typically occur around or exceed 10^3 Hz, which places them beyond the detection capabilities of upcoming GW observatories. Conversely, the GW spectrum linked with cosmic strings displays a relatively flat profile, particularly for larger v_φ. Specifically, for BP4, the GW signal can be detected by several future detectors such as LISA [29], TianQin [30], DECIGO [31], BBO [32] and CE [33].

3 Leptogenesis

During the bubble expansion, a given fraction of right-handed neutrinos can penetrate into the bubbles and then decay into

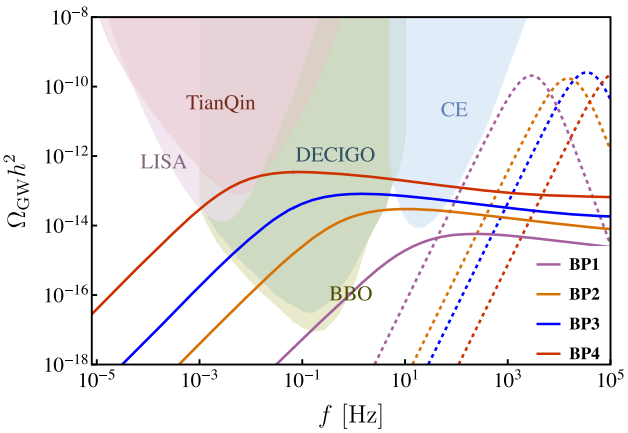

Fig. 1 GW signals emitted from cosmic strings (represented by solid lines) and during FOPT (represented by dashed lines) for four benchmark points are summarized in Table 1

the lepton asymmetry. In this study, the baryon asymmetry of the universe is generated by the decay of the second lightest right-handed neutrino ν_R^2, such that the lower bound on M_R^1 disappears and is replaced by a lower bound on M_R^2. The lifetime of ν_R^1 is proportional to $(M_R^1)^{-5}$ [34] and is sufficiently long for keV-scale right-handed neutrino to be the DM candidate. This scenario has been explored in various studies [35–38], which demonstrate that the mass of second lightest right-handed neutrino must satisfiy 10^9 GeV $\lesssim M_R^2 \lesssim 10^{12}$ GeV. We refer to ν_R^2 as N in the following discussions. The final baryonic asymmetry is then written as follows

$$Y_B = \epsilon_{CP}\kappa_{\rm sph}\kappa_{\rm pen}\kappa_{\rm dep}\kappa_{\rm wash}Y_N^{\rm eq}\left(\frac{T_n}{T_{\rm RH}}\right)^3. \tag{19}$$

where $Y_N^{\rm eq} \equiv n_N^{\rm eq}/s$ is the equilibrium abundance of right-handed neutrinos, ϵ_{CP} is the CP asymmetry of the decay of heavy right-handed neutrinos and $\kappa_{\rm sph} = 28/79$ is the fraction of lepton aymmetry that is converted into baryon asymmetry by electroweak sphalerons. Reheating temperature is defined by $T_{\rm RH} \simeq (1+\alpha)^{1/4}T_n$. $\kappa_{\rm pen}$ is the fraction that right-handed neutrinos penetrate into the bubbles. The $\kappa_{\rm dep}$ and the $(T_n/T_{\rm RH})^3$ account for the suppression comes from the process like $NN \to \varphi\varphi$ which depletes the RHN population and the reheating effects after phase transition respectively. $\kappa_{\rm wash}$ is the wash-out parameter induced by the inverse decay and scatterings. The bubble wall dynamics could help to enhance the factor $\kappa_{\rm wash}$ [39]. This works as follows: the penetrated RHNs are suddenly out of equilibrium if their masses satisfy $M_N \gg T_n$, then the wash-out effects are Boltzmann suppressed. This can often be realized in strong FOPT. Therefore, the required CP asymmetry is much smaller. However, the strong super-cooling FOPT also introduces extra suppression factor $\kappa_{\rm pen}(T_n/T_{\rm RH})^3$. It has been shown in Ref. [40] that the enhancement of bubble-assisted leptogenesis is maximized at $\alpha \sim 5$ and $M_N/T_{\rm RH} \gtrsim 7$, and the $B-L$ breaking scale could be reduced to $\mathcal{O}(10^9$ GeV) which can produce observational FOPT gravitational wave spectra.

Our work can not only take into account this bubble-assisted scenario, but also include extra contributions. The penetrated ν_R^2 could decay into lepton asymmetry in the usual way. Besides, the penetrated scalars Φ could also decay into leptons in terms of $\Phi \to \nu\nu$. We do not discuss the leptogenesis in details although we are motivated by it.

4 Lepton asymmetry and sterile neutrino DM

The field S undergoes the FOPT and subsequently induces the formation of the Q-balls from Φ. The Q-balls then decay into sterile neutrinos and lepton asymmetry stored for resonant production. Consequently, there are two primary mechanisms for neutrino genesis in this context: one is the decay of the Q-balls, and the other is the resonant oscillation process.

4.1 Q-balls from FOPT

Assuming the dark scalar Φ carries a good $U(1)$ symmetry like $U(1)_X$, the conserved number $N_\Phi - N_{\Phi^\dagger}$ can be packed by the true vacuum bubbles [41–45]. We do not focus on the origin of this primordial asymmetry in this work. At approximately $T_\star$, the false vacuum remnants shrink to the critical size $R_\star$. The "critical" means at this size there can not be another bubble nucleate in the false vacuum remnant, otherwise it will fission into more packets. This condition is expressed by:

$$\Gamma(T_\star)\frac{4\pi}{3}R_\star^3\Delta t \sim 1, \tag{20}$$

where $\Delta t = R_\star/v_w$ represents the time required for shrinking. The remnants shrink into Q-balls and the number density of Q-balls is given by:

$$n_Q^\star = \left(\frac{3}{4\pi}\right)^{1/4}\left(\frac{\Gamma(T_\star)}{v_w}\right)^{3/4}p(T_\star), \tag{21}$$

where we used the condition $\frac{4\pi}{3}R_\star^3 n_Q^\star = p(T_\star) = 0.29$ [44]. In a remnant, the trapped Q-charge is $Q_\star = F_{\rm trap}\eta_\Phi s_\star/n_Q^\star$ with $\eta_\Phi = n_\Phi/s$ being the primordial asymmetry and $s_\star = 2\pi^2 g_\star T_\star^3/45$ being the entropy density at $T_\star$. The trapping function $F_{\rm trap}$ depicts the fraction of particles that are trapped into the false vacuum. It depends on the bubble wall velocity v_w [46–49] and $m_\Phi/T_\star$ [50–52]. For $v_w = 0.6$ and $m_\Phi/T_\star = 10$, there are 96% of particles Φ being trapped inside the false vacuum. In this work, we set $F_{\rm trap} = 1$ for simplicity. And when all heavy particles Φ and $\Phi^\dagger$ are reflected, the upper limit of bubble wall velocity is given by [51]

$$\Delta V_{\rm eff} = \frac{\pi^2}{45}\frac{(1+v_w)^3}{1-v_w^2}T^4, \tag{22}$$

which can be rewritten by using $\Delta V_{\rm eff} \approx \alpha \times \rho_r$,

$$\alpha = \frac{2}{3g_\star}\frac{(1+v_w)^3}{1-v_w^2}. \tag{23}$$

For $\alpha = 0.5$ and $g_\star = 110$, the bubble wall velocity v_w is limited to less than 0.95. When we consider the FOPT happens in radiation dominated era and $T_\star \approx T_p$, the bounce action can be expressed as [53]:

$$\begin{aligned}\frac{S_3(T_\star)}{T_\star} &\approx 76 - 4\log\left(\frac{T_\star}{10^8\ {\rm GeV}}\right) - 4\log\left(\frac{\beta/H}{100}\right)\\ &\quad +3\log v_w - 2\log\left(\frac{g_\star}{100}\right),\end{aligned} \tag{24}$$

Then the initial charge of the Q-ball is

$$Q_\star \approx 1.12\times 10^{24}\times v_w^3\left(\frac{\eta_\Phi}{10^{-3}}\right)\left(\frac{g_\star}{100}\right)^{-1/2}\times\left(\frac{T_\star}{10^8\ \text{GeV}}\right)^{-3}\left(\frac{\beta/H}{100}\right)^{-3}, \tag{25}$$

Besides, it is convenient to rewrite the $\Delta V_{\text{eff}} \approx \alpha \times \rho_r(T_\star)$. The Q-ball parameters R_Q and m_Q are obtained by minimizing its energy $E(R) = \frac{\pi Q}{R} + \frac{4\pi}{3}R^3\Delta V_{\text{eff}}$,

$$R_Q = \left(\frac{Q}{4\Delta V_{\text{eff}}}\right)^{1/4}, \quad m_Q = \frac{4\sqrt{2}\pi}{3}Q^{3/4}\Delta V_{\text{eff}}^{1/4}, \tag{26}$$

The effective particle energy ω_Q inside a Q-ball is given by $\omega_Q \approx \pi/R_Q$:

$$\omega_Q \approx 1\ \text{TeV}\times\alpha^{1/4}v_w^{-3/4}\left(\frac{\eta_\Phi}{10^{-3}}\right)^{-1/4}\left(\frac{g_\star}{100}\right)^{3/8}\times\left(\frac{T_\star}{10^8\ \text{GeV}}\right)^{7/4}\left(\frac{\beta/H}{100}\right)^{3/4}, \tag{27}$$

After the Q-balls formation, it will decay into the neutrinos and sterile neutrinos. If $\omega_Q > 2m_\nu, 2m_{\nu_s}$, the decay process is kinetically allowable. We adopt the saturated Q-ball decay rate [54]:

$$\Gamma_Q \simeq \frac{1}{Q}\frac{\omega_Q^3}{96\pi^2}4\pi R_Q^2, \tag{28}$$

In our model, the Q-ball can decay into both neutrinos and sterile neutrinos. It has been demonstrated in Ref. [55] that when Q-ball decay is saturated, the branching ratio for particle production by Q-ball decay should correspond to the ratio of the rate for the elementary processes. Specifically, the decay widths for the elementary processes where free Φ particles decay into neutrinos and sterile neutrinos are given by $\Gamma(\Phi\to\nu\nu) = \frac{y_\nu^2 m_\Phi}{16\pi}$ and $\Gamma(\Phi\to\nu_s\nu_s) = \frac{y_s^2 m_\Phi}{16\pi}$, respectively. Then the branching ratio of Q-ball decaying into sterile neutrinos is $\text{BR}_s = \frac{\Gamma(\Phi\to\nu_s\nu_s)}{\Gamma(\Phi\to\nu\nu)+\Gamma(\Phi\to\nu_s\nu_s)} = \frac{y_s^2}{y_\nu^2+y_s^2}$. By using $dQ/dt = Q\Gamma_Q$, we obtain the evolution of the charge of Q-ball respect to time,

$$Q = Q_\star\left[1-\frac{(t-t_\star)}{\tau_Q}\right]^{4/5}, \tag{29}$$

with $\tau_Q = \frac{96Q_\star^{5/4}}{5\pi^2(4\Delta V_{\text{eff}})^{1/4}}$. For convenience, we approximate the percolation temperature $T_\star$ and reheating temperature T_{RH} as being equivalent to the nucleation temperature T_n due to the mild α. The decay temperature is given by

$$T_{\text{dec}} = \left(\frac{45}{4\pi^3 g_\star}\right)^{1/4}\sqrt{\Gamma_Q M_{\text{pl}}}, \tag{30}$$

which leads to

$$T_{\text{dec}} \simeq 10\ \text{MeV}\times\alpha^{1/8}v_w^{-15/8}\left(\frac{\eta_\Phi}{10^{-3}}\right)^{-5/8}\left(\frac{g_\star}{100}\right)^{3/16}\times\left(\frac{T_n}{10^8\text{GeV}}\right)^{19/8}\left(\frac{\beta/H}{100}\right)^{15/8}. \tag{31}$$

The decay temperature has to be larger than 4 MeV in order to avoid the BBN constraint [56]. The energy density ratio of Q-ball to radiation at T_{dec} is given by:

$$\left.\frac{n_Q m_Q}{\rho_r}\right|_{T_{\text{dec}}} = \frac{n_Q^\star m_Q}{\rho_r(T_n)}\frac{T_n}{T_{\text{dec}}} \simeq 191\times\alpha^{1/8}v_w^{9/8}\left(\frac{\eta_\Phi}{10^{-3}}\right)^{11/8}\times\left(\frac{g_\star}{100}\right)^{3/16}\left(\frac{T_n}{10^8\text{GeV}}\right)^{-5/8}\left(\frac{\beta/H}{100}\right)^{-9/8}, \tag{32}$$

which exceeds unity for the benchmark parameters, ensuring domination by the Q-ball.

For producing lepton asymmetry, the production has to avoid the electroweak sphaleron such that the decay temperature is restricted to be below the temperature of electroweak phase transition.

4.2 Lepton asymmetry

In this work, since the entropy density at T_{dec} is 4 $\left(n_Q(T_{\text{dec}})m_Q + \rho_r(T_{\text{dec}})\right)/3T_{\text{dec}}$, the lepton asymmetry comes from the Q-ball decay reads,

$$\eta_L \simeq 2\text{BR}_L\frac{3n_\Phi T_{\text{dec}}}{4\left(n_Q^\star m_Q + \rho_r(T_n)\frac{T_{\text{dec}}}{T_n}\right)} = \begin{cases} 2\times 10^{-3}\ \text{BR}_L\left(\frac{\eta_\Phi}{10^{-3}}\right), & \text{RD} \\ 10^{-5}\times\alpha^{-1/8}v_w^{-9/8}\text{BR}_L\left(\frac{\eta_\Phi}{10^{-3}}\right)^{-3/8} & \\ \times\left(\frac{g_\star}{100}\right)^{-3/16}\left(\frac{T_n}{10^8\ \text{GeV}}\right)^{5/8}\left(\frac{\beta/H}{100}\right)^{9/8}, & \text{QD} \end{cases} \tag{33}$$

where $\text{BR}_L = \sum_i (y_\nu^i)^2/\left(y_s^2 + \sum_i (y_\nu^i)^2\right)$ and $\text{BR}_s = 1 - \text{BR}_L$ are the branching ratio that decay into neutrinos and sterile neutrinos respectively. RD and QD represent the Q-ball decay in radiation dominated universe and Q-ball dominated universe respectively. We fix $\alpha = 0.5$, $v_w = 0.6$, $g_\star = 110$, $\beta/H = 100$ and the corresponding η_L is shown in Fig. 2. We can see that the maximal lepton asymmetry produced by Q-ball decay in the conformal $B-L$ model can only reach 0.0005. This is because the lepton asymmetry is proportional to $\alpha^{-1/8}(\beta/H)^{9/8}$ and the conformal model often predicts large α and small β/H. It needs to decrease the α and increase β/H for producing larger lepton asymmetry.

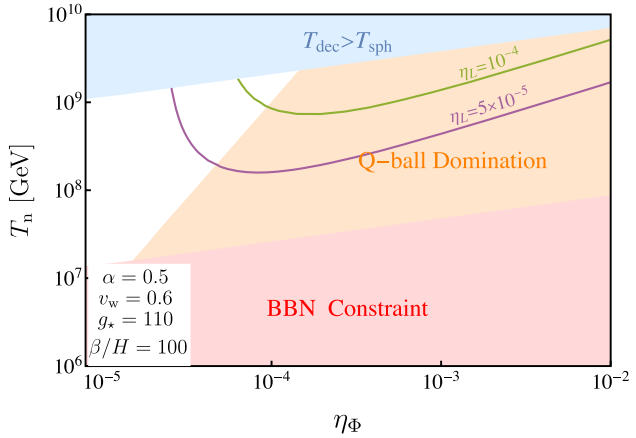

Fig. 2 Constraints on the nucleation temperature $T_{\rm n}$ and lepton asymmetry η_Φ in a Q-ball decay scenario. The upper bounds ensure that lepton asymmetry is sufficient for resonant production without conversion to baryon asymmetry through electroweak sphaleron processes, where $T_{\rm sph}\approx 100$GeV. The lower bound is based on the BBN constraint

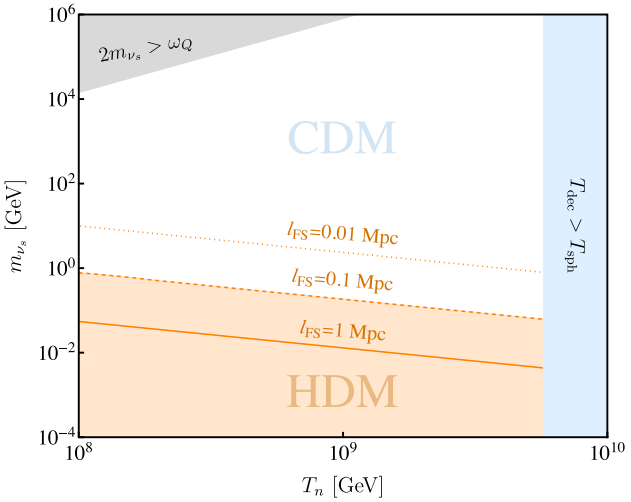

Fig. 3 Free-streaming length of sterile DM which is produced from Q-ball decay. Solid, dashed and dotted lines denote $l_{\rm FS}=1$ Mpc, $l_{\rm FS}=0.1$ Mpc and $l_{\rm FS}=0.01$ Mpc respectively. CDM and HDM denote "cold dark matter" and "hot dark matter" separately. The gray region represents $2m_{\nu_s}>\omega_Q$ where the Q-ball decay into sterile neutrinos is forbidden

4.3 Heavy sterile neutrino DM: Q-ball decay

The number densities of Q-ball and decayed particles sterile neutrino are related as follows

$$\frac{n_{\nu_s}(T_{\rm dec})}{s(T_{\rm dec})}=\frac{{\rm BR}_s}{{\rm BR}_L}\eta_L. \tag{34}$$

And the relic density of neutrino is:

$$\Omega_{\nu_s}^{\rm dec}h^2=\frac{n_{\nu_s}(T_0)m_{\nu_s}}{\rho_{\rm c}}h^2=\frac{n_{\nu_s}(T_{\rm dec})s(T_0)m_{\nu_s}}{s(T_{\rm dec})\rho_c}h^2, \tag{35}$$

the critical energy density, represented as $\rho_{\rm c}$, is defined as $3H_0^2M_{\rm Pl}^2/(8\pi)$, which is equivalent to $(2.5\times10^{-12}{\rm GeV})^4$. H_0 denotes the Hubble constant today, and $h=H_0/\left(100\,{\rm km\ s^{-1}\cdot Mpc^{-1}}\right)\approx 0.67$. Actually, there may also be contributions from the penetrated φ and Φ. Assuming the penetrated scalars is in thermal equilibrium through some portals like Higgs portal, in Ref. [57], it has been shown that the contribution to the sterile neutrino DM relic density from the decay of the scalars, when we neglect the reheating due to Q-ball decay, reads,

$$\Omega_{\nu_s}^{\Phi}h^2\simeq 8.64\times10^{-8}\times\left(\frac{{\rm BR_s}}{10^{-6}}\right)\left(\frac{m_{\nu_s}}{\rm GeV}\right)^3\left(\frac{10^8\ {\rm GeV}}{m_\varphi}\right)\times\left(\frac{10^8\ {\rm GeV}}{v_\varphi}\right)^2, \tag{36}$$

which should be negligible in this work.

If the sterile neutrinos from Q-ball decay compose all the observed DM, the free-streaming length is given by [58]

$$l_{\rm FS}\simeq 0.1\ {\rm Mpc}\left(\frac{3.36}{g_\star(T_{\rm NR})}\right)^{1/2}\left(\frac{3.91}{g_s(T_{\rm NR})}\right)^{-1/3}\left(\frac{\rm keV}{T_{\rm NR}}\right)\times\left[1+\log\left(\frac{T_{\rm NR}}{T_{\rm eq}}\right)+\frac{1}{4}\log\left(\frac{g_\star(T_{\rm NR})}{g_\star(T_{\rm eq})}\right)\right], \tag{37}$$

where $T_{\rm eq}\approx 3$ eV is the temperature at matter radiation equality and $g_s(T)$ is the effective number of relativistic entropy degrees of freedom. DM becomes non-relativistic when the DM momentum $p_{\nu_s}(T_{\rm NR})=(\omega_Q/2)[(g_s(T_{\rm NR})T_{\rm NR})/(g_s(T_{\rm dec})T_{\rm dec})]^{1/3}\simeq m_{\nu_s}$ and the corresponding temperature

$$\begin{aligned}T_{\rm NR}&=T_{\rm dec}\left(\frac{2m_{\nu_s}}{\omega_Q}\right)\left(\frac{g_s(T_{\rm NR})}{g_s(T_{\rm dec})}\right)^{-1/3}\\&=0.15\ {\rm eV}\left(\frac{m_{\nu_s}}{10\ {\rm keV}}\right)\left(\frac{g_s(T_{\rm NR})}{g_s(T_{\rm dec})}\right)^{-1/3}\alpha^{-1/8}v_w^{-9/8}\\&\quad\times\left(\frac{\eta_\Phi}{10^{-3}}\right)^{-3/8}\left(\frac{g_\star}{100}\right)^{-3/16}\left(\frac{T_n}{10^8{\rm GeV}}\right)^{5/8}\left(\frac{\beta/H}{100}\right)^{9/8},\end{aligned} \tag{38}$$

we set $g_\star(T_{\rm NR})=3.36$ and $g_s(T_{\rm NR})=3.91$ for $T_{\rm NR}<1$ MeV. The free-streaming length is shown in Fig. 3.

From Fig. 3 it can be seen that if the sterile neutrinos from Q-ball decay compose all the observed DM, the sterile neutrino mass has to satisfy

$$m_{\nu_s}\gtrsim 100\ {\rm MeV}. \tag{39}$$

4.4 keV sterile neutrino DM: oscillation production

The distribution of sterile neutrinos evolves in the universe according to the following formula [59]:

$$\frac{df_{\nu_s}}{dt} = \frac{\Gamma_{\nu_a}}{4}\sin^2 2\theta_M \left(f_{\nu_a} - f_{\nu_s}\right), \tag{40}$$

where $\Gamma_{\nu_a} = y_a(T)G_F^2 pT^4$ is the thermal width of the active neutrinos with G_F and $y_a(T)$ being the Fermi coupling constant and prefactor that depends on the temperature of universe separately, then

$$\sin^2 2\theta_M \simeq \frac{\Delta^2 \sin^2 2\theta}{\Delta^2 \sin^2 2\theta + \Gamma_{\nu_a}^2/4 + (\Delta\cos 2\theta - V_a)^2}, \tag{41}$$

with $\Delta \approx \frac{m_{\nu_s}^2}{2p}$ and $\theta \simeq m_\nu/m_{\nu_s}$ is the mixing angle in vacuum. The thermal self-energy of neutrinos and anti-neutrinos, V_a and $V_{\bar{a}}$, can be expressed as [60,61]:

$$V_{a,\bar{a}} = \pm\sqrt{2}G_{\rm F}\left(2\eta_{\nu_a} + \sum_{b\neq a}\eta_{\nu_b}\right)s(T) - B_a q T^5, \tag{42}$$

where $q = \frac{p}{T}$, $s(T)$ denotes the entropy density at temperature T and a, b refer to the flavors of neutrinos, B_a is a constant valued at 10.88×10^{-9} GeV^{-4} for $a = e$ [62].

Using $\theta \approx 0$, the total sterile neutrinos follows the relation:

$$\frac{{\rm d}f_{\nu_s}}{{\rm d}t} = \frac{\Gamma_{\nu_a} m_{\nu_s}^4 \sin^2 2\theta}{16p^2}\left(\frac{f_{\nu_a}}{\omega_{\rm eff}^2} + \frac{f_{\bar{\nu}_a}}{\bar{\omega}_{\rm eff}^2}\right), \tag{43}$$

Here, we make the approximation $f_{\nu_a}, f_{\bar{\nu}_a} \gg f_{\nu_s}$, and define $\omega_{\rm eff}^2 = (\frac{m_{\nu_s}^2}{2p} - V_a)^2 + \frac{\Gamma_{\nu_a}^2}{4}$ and $\bar{\omega}_{\rm eff}^2 = \left(\frac{m_{\nu_s}^2}{2p} - V_{\bar{a}}\right)^2 + \frac{\Gamma_{\nu_a}^2}{4}$.

We follow the general approach to solve the Boltzmann equation by defining a dimensionless co-moving momentum $\xi = \left(\frac{g_s(T_i)}{g_s(T)}\right)^{\frac{1}{3}} q$, and T_i denotes the reference temperature. To determine the distribution function for sterile neutrinos, we postulate that the active neutrinos maintain thermal equilibrium and obey the Fermi-Dirac distribution. Our analysis focuses solely on the oscillation between electron neutrinos and sterile neutrinos, as follows:

$$f_{\nu_e,\bar{\nu}_e}(\xi, T) = 1/\left[1 + \exp\left(q \mp \frac{4\pi^2}{15}g_s(T)\eta_{\nu_e}(T)\right)\right]. \tag{44}$$

Here we consider the initial lepton asymmetry $\eta_{\nu_e}^{\rm ini} \approx \eta_L$ and the time evolution of η_{ν_e} is given by [61,63]:

$$\frac{\rm d}{{\rm d}t}\eta_{\nu_e}(T) = -\frac{45 m_{\nu_s}^4 \sin^2 2\theta}{64\pi^4 g_s(T_i)}\int {\rm d}\xi\,\xi^2 \frac{\Gamma_{\nu_e}(\xi, T)}{p^2} \times\left(\frac{f_{\nu_e}(\xi, T)}{\omega_{\rm eff}^2(\xi, T)} - \frac{f_{\bar{\nu}_e}(\xi, T)}{\bar{\omega}_{\rm eff}^2(\xi, T)}\right). \tag{45}$$

In order to solve the Eqs. (43) and (45) numerically, we should utilize the time-temperature relation, which reads:

$$\frac{{\rm d}t}{{\rm d}T} = -\sqrt{\frac{45}{4\pi^3 g_\star(T)}}\frac{M_{\rm pl}}{T^3}\left(1 + \frac{1}{3}\frac{g_s'(T)}{g_s(T)}\right), \tag{46}$$

the prime notation represents differentiation with respect to temperature. Utilizing fitting formulas cited in Ref. [64], we calculated how the effective number of relativistic entropy degrees of freedom, $g_s(T)$, and its rate of change, $g_s'(T)$, evolve with temperature.

Therefore, the relic abundance of sterile neutrinos from oscillation part can be obtained by:

$$\Omega_{\nu_s}^{\rm osc}h^2 = \frac{m_{\nu_s}h^2 T_0^3}{\rho_{\rm c}}\frac{g_s(T_0)}{g_s(T_i)}\int\frac{{\rm d}\xi}{2\pi^2}\xi^2 f_{\nu_s}\left(\xi, T = T_f\right), \tag{47}$$

where we choose $T_f = 100$ keV as the final temperature in numerical calculation. If the sterile neutrino DM is produced by the pure resonant active-sterile neutrino oscillation, in Ref. [63] the constraint from Lyman-α can be evaded when the sterile neutrino mass fulfills the relation $m_{\nu_s} \gtrsim 8.4$ keV. This is reconsidered in Ref. [61], $m_{\nu_s} \gtrsim 18$ keV for $\eta_\Phi \gtrsim 10^{-4}$.

From Eqs. (37) and (38) it is easy to see that for $m_{\nu_s} \sim \mathcal{O}(10\,{\rm keV})$, $l_{\rm FS} \gg 0.1$ Mpc and the DM from Q-ball decay is hot. In this case, the contribution of sterile neutrino DM from Q-ball decay must be subdominant. Besides, these hot DM behaves like dark radiation in the early stage after Q-ball decay. They contribute to the effective number of neutrino species [65],

$$\Delta N_{\rm eff} = \frac{\rho_{\nu_s}\left(T_{\rm eq}\right)}{\rho_r\left(T_{\rm eq}\right)}\left[N_\nu + \frac{8}{7}\left(\frac{11}{4}\right)^{4/3}\right], \tag{48}$$

where $N_\nu = 3.045$ in the standard model [66,67] and $\rho_{\nu_s}\left(T_{\rm eq}\right)/\rho_r\left(T_{\rm eq}\right) \approx {\rm BR}_s$. Further, Q-ball decay sterile neutrinos can also contribute to total sterile neutrino abundance, thus $\Omega_{\nu_s}h^2 = \Omega_{\nu_s}^{\rm dec}h^2 + \Omega_{\nu_s}^{\rm osc}h^2$. Because the sterile neutrinos from decay are hot, we set $\Omega_{\nu_s}^{\rm dec}h^2/0.12 \lesssim 0.1$ for simplicity. Since the decay contribution must be sub-dominate in this case, we fix $\Omega_{\nu_s}^{\rm dec}h^2 \equiv 0.012$ here.

We assume the sterile neutrino DM gives the Majorana mass of the lightest neutrino ν_1 through the seesaw mechanism, $m_{\nu_1} = m_D^2/m_{\nu_s}$. Based on neutrino oscillation data, the best fit values for the mass-splittings are $m_{\nu_2} - m_{\nu_1} \approx 0.0085$ eV and $m_{\nu_3} - m_{\nu_1} \approx 0.05$ eV, assuming a normal hierarchy of neutrino masses [68]. Additionally, cosmological data constrain the sum of the three neutrino masses to $\sum_i m_{\nu_i} < 0.118$ eV [69]. These constraints suggest that $m_{\nu_1} < 0.02$ eV, although the exact value remains undetermined. Consequently, we derive that $\sin^2 2\theta \approx 4m_D^2/m_{\nu_s}^2 \approx 4m_{\nu_1}/m_{\nu_s} < \frac{0.08\,{\rm eV}}{m_{\nu_s}} < 10^{-5}$. We only get an upper bound of $\sin^2 2\theta$ and thus treat it as a free parameter in this work. We present the $m_s - \sin^2 2\theta$ contour in Fig. 4 to illustrate in explaining all DM with corresponding X-ray limitation.

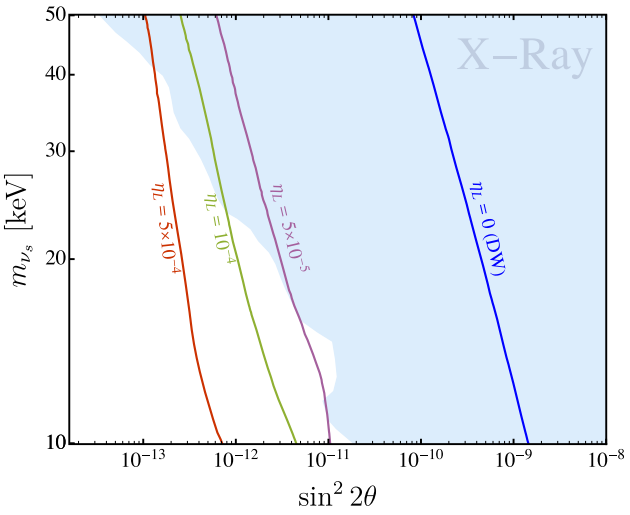

Fig. 4 The panel displaying $\sin^2 2\theta$ and m_{ν_s} elucidates the compatibility of $\Omega_{\nu_s}h^2 \equiv 0.12$. The blue region is ruled out by the X-ray constraints [70]

We observe that $\eta_L \geq 5 \times 10^{-5}$ is required to evade X-ray constraints at least.

5 Conclusion

In this paper, we have explored two types of sterile DM associated with large lepton asymmetry, assisted by Q-ball decay during the FOPT of the $U(1)_{B-L}$ model. Q-balls form during the FOPT by trapping the number-conserved particles into the false vacuum. We analyzed the GWs emitted throughout the process. GWs originating from the FOPT are difficult to detect due to their high peak frequencies. In contrast, GWs produced following $U(1)_{B-L}$ symmetry breaking, particularly for larger vacuum values v_φ, are within the detection capabilities of future GW observatories, including LISA, TianQin, BBO, DECIGO and CE.

For the two types of sterile DM, the first type involves heavy sterile DM, with masses exceeding 100 MeV; the second consists of keV sterile neutrino DM, produced resonantly with the aid of Q-ball decay, which provides the requisite lepton asymmetry. Additionally, small amounts of keV sterile neutrino DM can also be produced directly by Q-ball decay.

Acknowledgements We thank Ahmad Mohamadnejad, Ki-Young Choi and Cristina Benso for useful discussions and Jing Yang for helpful suggestions on the manuscript. This work is supported by Scientific Research Foundation of Inner Mongolia University under grant No.10000-22311201/036 and Scientific Research Foundation of Inner Mongolia Autonomous Region under grant No.12000-15042261.

Data Availability Statement This manuscript has no associated data. [Authors' comment: This is a theoretical study and no experimental data has been listed.]

Code Availability Statement The manuscript has no associated code/software. [Author's comment: Code/Software sharing not applicable to this article as no code/software was generated or analysed during the current study.]

Funded by SCOAP[3].

Appendix A: Zero-temperature potential

The one-loop contributions from Z', ν_R^i and Φ induce a Colman–Weinberg potential [71,72]

$$V_{\rm CW}^1 = \frac{1}{64\pi^2}\sum_{k=1}^{n}(-1)^{n_f} n_k m_k(\varphi)^4 \left(\log\frac{m_k(\varphi)^2}{\Lambda^2} - C_k\right), \tag{A1}$$

where $C_k = 3/2$ (5/6) for scalars/spinors (vectors). Λ is the renormalization group (RG) scale. We can substitute the field dependent mass $m_k(\varphi) \to \frac{M_k}{v_\varphi}\varphi$, where M_k is the measured mass of particle k,

$$M_{Z'} = 2g_{B-L}v_\varphi, \quad M_i = y_{R,i}\frac{v_\varphi}{\sqrt{2}}, \quad M_S = \frac{\sqrt{\lambda_{\phi s}}}{\sqrt{2}}v_\varphi. \tag{A2}$$

substituting in Eq. (A1) results the well-known Gildener–Weinberg formula [73]

$$V_{\rm GW}^1 = A\varphi^4 + B\varphi^4\log\frac{\varphi^2}{\Lambda^2}, \tag{A3}$$

where

$$\begin{aligned} A &= \frac{1}{64\pi^2 v_\varphi^4}\sum_{k=1}^{n} g_k M_k^4\left(\log\frac{M_k^2}{v_\varphi^2} - C_k\right), \\ B &= \frac{1}{64\pi^2 v_\varphi^4}\sum_{k=1}^{n} g_k M_k^4. \end{aligned} \tag{A4}$$

The total zero-temperature potential then reads

$$V_0 = \left(A + \frac{\lambda_s}{4}\right)\varphi^4 + B\varphi^4\log\frac{\varphi^2}{\Lambda^2}, \tag{A5}$$

To find the true vacuum, one should find the minimum of the potential (A5), given by

$$\langle\varphi\rangle = v_\varphi = \Lambda e^{-\left(\frac{4A+\lambda_s}{8B}+\frac{1}{4}\right)}, \tag{A6}$$

Combining this with Eq. (A5) we can substitute RG scale Λ and get:

$$V_0 = B_1\varphi^4\left(\log\frac{\varphi}{v_\varphi} - \frac{1}{4}\right), \tag{A7}$$

where

$$B_1 = \frac{3}{2\pi^2}\left(\frac{\lambda_{\phi s}^2}{96} + g_{B-L}^4 - \sum_i \frac{y_{R,i}^4}{96}\right). \tag{A8}$$

Appendix B: GWs during FOPT

The GW signals of a FOPT mainly comes from three sources: bubble collision, sound wave and turbulence. The GW spectra from bubble collision is given by [74,75]

$$\Omega_{\rm co}(f)h^2 \simeq 1.67\times10^{-5}\left(\frac{H}{\beta}\right)^2\left(\frac{\kappa_b\alpha}{1+\alpha}\right)^2\left(\frac{100}{g_\star}\right)^{1/3} \times\frac{0.11v_w^3}{0.42+v_w^2}\frac{3.8\,(f/f_{\rm co})^{2.8}}{1+2.8\,(f/f_{\rm co})^{3.8}}, \tag{B1}$$

where κ_b denotes the fraction of vacuum energy converted into the wall kinetic energy. The peak frequency of bubble collision processes is:

$$f_{\rm co} \simeq 1.65\times10^{-5}\,{\rm Hz}\left(\frac{\beta}{H}\right)\left(\frac{0.62}{1.8-0.1v_w+v_w^2}\right) \times\left(\frac{T_{\rm RH}}{100\,{\rm GeV}}\right)\left(\frac{g_\star}{100}\right)^{1/6}. \tag{B2}$$

where $T_{\rm RH}$ is the reheating temperature which is defined by $T_{\rm RH} \simeq (1+\alpha)^{1/4}T_n$. GW spectrum from sound waves is [76]:

$$\Omega_{\rm sw}(f)h^2 \simeq 2.65\times10^{-6}\Upsilon_{\rm sw}\left(\frac{H}{\beta}\right)\left(\frac{\kappa_f\alpha}{1+\alpha}\right)^2\left(\frac{100}{g_\star}\right)^{1/3} \times v_w\,(f/f_{\rm sw})^3\left(\frac{7}{4+3\,(f/f_{\rm sw})^2}\right)^{7/2}, \tag{B3}$$

where κ_f represents the fraction of vacuum energy that transfers into sound waves. The peak frequency is:

$$f_{\rm sw} \simeq 1.9\times10^{-5}\,{\rm Hz}\frac{1}{v_w}\left(\frac{\beta}{H}\right)\left(\frac{T_{\rm RH}}{100\,{\rm GeV}}\right)\left(\frac{g_\star}{100}\right)^{1/6}. \tag{B4}$$

We have included the suppression factor of the short period of the sound wave [77]

$$\Upsilon_{\rm sw} = \left(1-\frac{1}{\sqrt{1+2\tau_{\rm sw}H}}\right), \tag{B5}$$

where

$$\tau_{\rm sw}H \approx (8\pi)^{\frac{1}{3}}\frac{v_wH}{\beta\sqrt{3\kappa_v\alpha/(4+4\alpha)}}. \tag{B6}$$

The formula of the stochastic gravitational wave background spectrum from turbulence is [78]:

$$\Omega_{\rm turb}(f)h^2 \simeq 3.35\times10^{-4}\left(\frac{Hv_w}{\beta}\right)\left(\frac{\kappa_{\rm turb}\alpha}{1+\alpha}\right)^{3/2}\left(\frac{100}{g_\star}\right)^{1/3} \times\frac{(f/f_{\rm turb})^3}{(1+f/f_{\rm turb})^{11/3}\left(1+8\pi f/h_p\right)}, \tag{B7}$$

and h_p is expressed as:

$$h_p = 1.65\times10^{-5}\,{\rm Hz}\left(\frac{T_{\rm RH}}{100\,{\rm GeV}}\right)\left(\frac{g_\star}{100}\right)^{\frac{1}{6}}, \tag{B8}$$

where

$$\kappa_{\rm turb} = \tilde{\epsilon}\kappa_f, \tag{B9}$$

We set $\tilde{\epsilon} = 0.1$. The peak frequency of gravitational wave from turbulence processes is given by:

$$f_{\rm turb} \simeq 2.7\times10^{-5}\,{\rm Hz}\frac{1}{v_w}\left(\frac{\beta}{H}\right)\left(\frac{T_{\rm RH}}{100\,{\rm GeV}}\right)\left(\frac{g_\star}{100}\right)^{1/6}. \tag{B10}$$

The total contribution to the SGWB can be calculated by integrating these individual contributions:

$$\Omega_{\rm GW}(f)h^2 = \Omega_{\rm co}(f)h^2 + \Omega_{\rm sw}(f)h^2 + \Omega_{\rm turb}(f)h^2. \tag{B11}$$

Further, we consider the redshift effect of the GW induced by Q-ball domination and define a dimensionless redshift factor $R \simeq \frac{T_{\rm dom}}{T_{\rm dec}}$, with $T_{\rm dom} \simeq \frac{n_Q^\star m_Q}{\rho_r(T_n)}T_n$. The form of R follows:

$$R \simeq 188\times\alpha^{1/8}v_w^{9/8}\left(\frac{\eta_\Phi}{10^{-3}}\right)^{11/8}\left(\frac{g_\star}{100}\right)^{-7/48} \times\left(\frac{T_n}{10^8{\rm GeV}}\right)^{-5/8}\left(\frac{\beta/H}{100}\right)^{-9/8}. \tag{B12}$$

The peak frequency and the spectra will redshift as $f'_{\rm peak} = \frac{f_{\rm peak}}{R^{1/3}}$ and $\Omega'_{\rm GW} = \frac{\Omega_{\rm GW}}{R^{4/3}}$. However, we found for benchmark points the dominating effect of Q-balls is not significant enough to impact the shape of the spectra significantly, so we neglect these redshift effects.

Appendix C: GWs emitted from cosmic strings

Cosmic strings, one-dimensional defects, arise during spontaneous symmetry breaking phase transition in the early universe. Particularly, we mainly consider Nambu-Goto cosmic strings that form subsequent to the $U(1)_{B-L}$ symmetry breaking. Cosmic strings interact and collide to form smaller, self-contained loops that emit GWs via cusps, kinks, and kink-kink collisions.

Generally, The total power emitted in gravitational wave by string loops can be described by quadrupole formula, $P_{\rm total} = \Gamma_s G\mu^2$, G is the gravitational constant and $\mu \sim v_\varphi^2$

denotes the energy density per unit length. Γ_s always be 50 through huge numerical simulation [79,80]. To account for the dilution and expansion of the universe, the gravitational wave energy density spectrum emitted by a network of cosmic strings is modeled as follows [81]:

$$\frac{d\rho_{\mathrm{GW}}(t)}{df}=\int^{t}dt'\frac{a\left(t'\right)^{4}}{a(t)^{4}}\int dl\frac{dn_{\mathrm{cs}}\left(l,t'\right)}{dl}\frac{dP_{\mathrm{GW}}\left(l,t'\right)}{df'}\frac{df'}{df}, \tag{C1}$$

and

$$\frac{df'}{df}=\frac{a(t)}{a\left(t'\right)},\quad \frac{dn_{\mathbf{cs}}}{dl}\left(l,t'\right)=\frac{dn_{\mathrm{cs}}}{dt_k}\frac{dt_k}{dl}, \tag{C2}$$

$$\frac{dP_{\mathrm{GW}}\left(l,t'\right)}{df'}=\Gamma_s G\mu^2 lj\left(f\frac{a(t)}{a\left(t'\right)}l\right), \tag{C3}$$

here, f' is the emission frequency, $a(t)$ is the scale factor, $n_{\mathrm{cs}}(l,t)$ denotes the number density of the string loops of length l and $P_{\mathrm{GW}}(l,f)$ is the power spectrum of GW with frequency f emitted by a loop of length l. Loops are formed with a length $l_k\approx\gamma t_k$, where t_k is the time of formation and γ is a constant valued at 0.1 [80,82], as determined by simulation. Besides, since the loops will lose energy when emit GW outside, we can obtain the relation between loops length and formation time: $l=\gamma t_k-\Gamma_s G\mu(t-t_k)$. Then, The loop number density production rate obtained from simulation [83–85]:

$$\frac{dn_{\mathrm{cs}}}{dt_k}=\left(\frac{\mathcal{F}C_{\mathrm{eff}}\left(t_k\right)}{\gamma t_k^4}\frac{a\left(t_k\right)^3}{a(t)^3}\right), \tag{C4}$$

where $C_{\mathrm{eff}}=5.4$ [86] represents the loop formation efficiency in radiation domination epoch and $\mathcal{F}=0.1$ [82] is energy conversion rate from infinite string network into loops of size l_k. Furthermore, the harmonics number n labels the radiation frequency $f=n/\frac{l}{2}$. The corresponding power spectrum for the discrete spectrum reads [83]:

$$j(x)=\sum_n\mathcal{P}_n\delta(x-2n), \tag{C5}$$

and the average power in nth mode $\mathcal{P}_n$ follows the form $\mathcal{P}_n=\frac{n^{-\frac{4}{3}}}{\zeta(\frac{4}{3})}$ [87] with $\zeta(\frac{4}{3})$ being 3.6. According to Eqs. (C1)–(C5), the stochastic GW spectrum is (t_0 is the current cosmic time and t_{form} refers to the initial formation time):

$$\begin{aligned}\Omega_{\mathrm{GW}}(f)h^2&\equiv\frac{h^2}{\rho_c}\frac{d\rho_{\mathrm{GW}}}{d\log f}\\&=\frac{8\pi h^2}{3H_0^2}\frac{\Gamma_s G^2\mu^2}{\gamma+\Gamma_s G\mu}\sum_{n=1}^{\infty}\frac{2n}{f}\int_{t_{\mathrm{form}}}^{t_0}dt\left(\frac{a(t)}{a\left(t_0\right)}\right)^5\\&\quad\times\left(\frac{\mathcal{F}C_{\mathrm{eff}}\left(t_k\right)}{\gamma t_k^4}\frac{a\left(t_k\right)^3}{a(t)^3}\right)\mathcal{P}_n.\end{aligned} \tag{C6}$$

References

1. M. Drewes et al., A white paper on keV sterile neutrino dark matter. JCAP **01**, 025 (2017)
2. S. Davidson, E. Nardi, Y. Nir, Leptogenesis. Phys. Rep. **466**, 105–177 (2008)
3. S. Dodelson, L.M. Widrow, Sterile-neutrinos as dark matter. Phys. Rev. Lett. **72**, 17–20 (1994)
4. K. Abazajian, S.M. Koushiappas, Constraints on sterile neutrino dark matter. Phys. Rev. D **74**, 023527 (2006)
5. X.-D. Shi, G.M. Fuller, A New dark matter candidate: nonthermal sterile neutrinos. Phys. Rev. Lett. **82**, 2832–2835 (1999)
6. A. Kusenko, Sterile neutrinos, dark matter, and the pulsar velocities in models with a Higgs singlet. Phys. Rev. Lett. **97**, 241301 (2006)
7. K. Petraki, A. Kusenko, Dark-matter sterile neutrinos in models with a gauge singlet in the Higgs sector. Phys. Rev. D **77**, 065014 (2008)
8. A. Merle, V. Niro, D. Schmidt, New production mechanism for keV sterile neutrino dark matter by decays of frozen-in scalars. JCAP **03**, 028 (2014)
9. A. Adulpravitchai, M.A. Schmidt, A fresh look at keV sterile neutrino dark matter from frozen-in scalars. JHEP **01**, 006 (2015)
10. M. Chen, G.B. Gelmini, L. Philip, V. Takhistov, Primordial black hole neutrinogenesis of sterile neutrino dark matter. Phys. Lett. B **852**, 138609 (2024)
11. L. Canetti, M. Drewes, T. Frossard, M. Shaposhnikov, Dark matter, baryogenesis and neutrino oscillations from right handed neutrinos. Phys. Rev. D **87**, 093006 (2013)
12. L. Canetti, M. Drewes, M. Shaposhnikov, Sterile neutrinos as the origin of dark and baryonic matter. Phys. Rev. Lett. **110**(6), 061801 (2013)
13. S. Eijima, M. Shaposhnikov, I. Timiryasov, Freeze-in and freeze-out generation of lepton asymmetries after baryogenesis in the νMSM. JCAP **04**(04), 049 (2022)
14. D. Borah, A. Dasgupta, Large neutrino asymmetry from TeV scale leptogenesis. Phys. Rev. D **108**(3), 035015 (2023)
15. Y.L. ChoeJo, K. Enomoto, Y. Kim, H.-S. Lee, Second leptogenesis: unraveling the baryon-lepton asymmetry discrepancy. JHEP **03**, 003 (2024)
16. M. Kawasaki, K. Murai, Lepton asymmetric universe. JCAP **08**(08), 041 (2022)
17. J.M. Berryman, A. De Gouvêa, K.J. Kelly, Y. Zhang, Lepton-number-charged scalars and neutrino beamstrahlung. Phys. Rev. D **97**(7), 075030 (2018)
18. X. Xun-Jie, S. Zhou, J. Zhu, The ν_R-philic scalar dark matter. JCAP **04**, 012 (2024)
19. I. Vilja, Baryogenesis in the singlet majoron model. Phys. Lett. B **324**, 197–200 (1994)
20. K. Enqvist, K. Kainulainen, I. Vilja, Phase transitions in the singlet majoron model. Nucl. Phys. B **403**, 749–769 (1993)
21. S. Iso, N. Okada, Y. Orikasa, Classically conformal B^- L extended Standard Model. Phys. Lett. B **676**, 81–87 (2009)
22. A. Das, N. Okada, N. Papapietro, Electroweak vacuum stability in classically conformal B-L extension of the Standard Model. Eur. Phys. J. C **77**(2), 122 (2017)
23. R.R. Parwani, Resummation in a hot scalar field theory. Phys. Rev. D **45**, 4695 (1992) (**Erratum: Phys. Rev. D 48, 5965 (1993)**)
24. B.A. Peter, E. Olivier, The effective potential and first order phase transitions: beyond leading-order. Phys. Rev. D **47**, 3546 (1993) (**Erratum: Phys. Rev. D 50, 6662 (1994)**)
25. A. Salvio, A. Strumia, N. Tetradis, A. Urbano, On gravitational and thermal corrections to vacuum decay. JHEP **09**, 054 (2016)
26. M.S. Turner, E.J. Weinberg, L.M. Widrow, Bubble nucleation in first order inflation and other cosmological phase transitions. Phys. Rev. D **46**, 2384–2403 (1992)

27. X. Wang, F.P. Huang, X. Zhang, Phase transition dynamics and gravitational wave spectra of strong first-order phase transition in supercooled universe. JCAP **05**, 045 (2020)
28. C.L. Wainwright, CosmoTransitions: computing cosmological phase transition temperatures and bubble profiles with multiple fields. Comput. Phys. Commun. **183**, 2006–2013 (2012)
29. P. Amaro-Seoane et al., Laser Interferometer Space. Antenna. **2**, (2017)
30. Z.-C. Liang, Z.-Y. Li, J. Cheng, E.-K. Li, J. Zhang, H. Yi-Ming, Impact of combinations of time-delay interferometry channels on stochastic gravitational wave background detection. Phys. Rev. D **107**(8), 083033 (2023)
31. S. Kawamura et al., Current status of space gravitational wave antenna DECIGO and B-DECIGO. PTEP **2021**(5), 05A105 (2021)
32. G.M. Harry, P. Fritschel, D.A. Shaddock, W. Folkner, E.S. Phinney, Laser interferometry for the big bang observer. Class. Quantum Gravity **23**, 4887–4894 (2006) (**Erratum: Class. Quant. Grav. 23, 7361 (2006)**)
33. D. Reitze et al., Cosmic explorer: the US contribution to gravitational-wave astronomy beyond LIGO. Bull. Am. Astron. Soc. **51**(7), 035 (2019)
34. A.D. Dolgov, S.H. Hansen, Massive sterile neutrinos as warm dark matter. Astropart. Phys. **16**, 339–344 (2002)
35. P. Di Bari, Seesaw geometry and leptogenesis. Nucl. Phys. B **727**, 318–354 (2005)
36. T. Asaka, S. Blanchet, M. Shaposhnikov, The nuMSM, dark matter and neutrino masses. Phys. Lett. B **631**, 151–156 (2005)
37. S. Antusch, P. Di Bari, D.A. Jones, S.F. King, A fuller flavour treatment of N_2-dominated leptogenesis. Nucl. Phys. B **856**, 180–209 (2012)
38. E. Bertuzzo, P. Di Bari, L. Marzola, The problem of the initial conditions in flavoured leptogenesis and the tauon N_2-dominated scenario. Nucl. Phys. B **849**, 521–548 (2011)
39. P. Huang, K.-P. Xie, Leptogenesis triggered by a first-order phase transition. JHEP **09**, 052 (2022)
40. E.J. Chun, T.P. Dutka, T.H. Jung, X. Nagels, M. Vanvlasselaer, Bubble-assisted leptogenesis. JHEP **09**, 164 (2023)
41. E. Krylov, A. Levin, V. Rubakov, Cosmological phase transition, baryon asymmetry and dark matter Q-balls. Phys. Rev. D **87**(8), 083528 (2013)
42. H.F. Peng, S.L. Chong, Probing the baryogenesis and dark matter relaxed in phase transition by gravitational waves and colliders. Phys. Rev. D **96**(9), 095028 (2017)
43. S. Jiang, A. Yang, J. Ma, F.P. Huang, Implication of nano-Hertz stochastic gravitational wave on dynamical dark matter through a dark first-order phase transition. Class. Quantum Gravity **41**(6), 065009 (2024)
44. J.-P. Hong, S. Jung, K.-P. Xie, Fermi-ball dark matter from a first-order phase transition. Phys. Rev. D **102**(7), 075028 (2020)
45. J. Siyu, H.F. Peng, K. Pyungwon, Gauged Q-ball dark matter through a cosmological first-order phase transition. 4 (2024)
46. G.D. Moore, T. Prokopec, How fast can the wall move? A Study of the electroweak phase transition dynamics. Phys. Rev. D **52**, 7182–7204 (1995)
47. S. Jiang, F.P. Huang, X. Wang, Bubble wall velocity during electroweak phase transition in the inert doublet model. Phys. Rev. D **107**(9), 095005 (2023)
48. B. Laurent, J.M. Cline, First principles determination of bubble wall velocity. Phys. Rev. D **106**(2), 023501 (2022)
49. W.-Y. Ai, B. Garbrecht, C. Tamarit, Bubble wall velocities in local equilibrium. JCAP **03**(03), 015 (2022)
50. M.J. Baker, J. Kopp, A.J. Long, Filtered dark matter at a first order phase transition. Phys. Rev. Lett. **125**(15), 151102 (2020)
51. D. Chway, T.H. Jung, C.S. Shin, Dark matter filtering-out effect during a first-order phase transition. Phys. Rev. D **101**(9), 095019 (2020)
52. S. Jiang, F.P. Huang, C.S. Li, Hydrodynamic effects on the filtered dark matter produced by a first-order phase transition. Phys. Rev. D **108**(6), 063508 (2023)
53. S.J. Huber, T. Konstandin, Production of gravitational waves in the nMSSM. JCAP **05**, 017 (2008)
54. A.G. Cohen, S.R. Coleman, H. Georgi, A. Manohar, The evaporation of Q balls. Nucl. Phys. B **272**, 301–321 (1986)
55. S. Kasuya, M. Kawasaki, M. Yamada, Revisiting the gravitino dark matter and baryon asymmetry from Q-ball decay in gauge mediation. Phys. Lett. B **726**, 1–7 (2013)
56. P.F. de Salas, M. Lattanzi, G. Mangano, G. Miele, S. Pastor, O. Pisanti, Bounds on very low reheating scenarios after Planck. Phys. Rev. D **92**(12), 123534 (2015)
57. H. Matsui, M. Nojiri, Higgs sector extension of the neutrino minimal standard model with thermal freeze-in production mechanism. Phys. Rev. D **92**(2), 025045 (2015)
58. K.-Y. Choi, J.-O. Gong, J. Joh, W.-I. Park, O. Seto, Light cold dark matter from non-thermal decay. Phys. Lett. B **845**, 138126 (2023)
59. K. Abazajian, G.M. Fuller, M. Patel, Sterile neutrino hot, warm, and cold dark matter. Phys. Rev. D **64**, 023501 (2001)
60. D. Notzold, G. Raffelt, Neutrino dispersion at finite temperature and density. Nucl. Phys. B **307**, 924–936 (1988)
61. K. Kentaro, K. Masahiro, M. Kai, Affleck-dine leptogenesis scenario for resonant production of sterile neutrino dark matter. 2 (2024)
62. G.B. Gelmini, L. Philip, V. Takhistov, Cosmological dependence of non-resonantly produced sterile neutrinos. JCAP **12**, 047 (2019)
63. M. Laine, M. Shaposhnikov, Sterile neutrino dark matter as a consequence of nuMSM-induced lepton asymmetry. JCAP **06**, 031 (2008)
64. O. Wantz, E.P.S. Shellard, Axion cosmology revisited. Phys. Rev. D **82**, 123508 (2010)
65. D. Hooper, G. Krnjaic, S.D. McDermott, Dark radiation and superheavy dark matter from black hole domination. JHEP **08**, 001 (2019)
66. P.F. de Salas, S. Pastor, Relic neutrino decoupling with flavour oscillations revisited. JCAP **07**, 051 (2016)
67. M.E. Abenza, Precision early universe thermodynamics made simple: $N_{\rm eff}$ and neutrino decoupling in the Standard Model and beyond. JCAP **05**, 048 (2020)
68. P.F. de Salas, D.V. Forero, S. Gariazzo, P. Martínez-Miravé, O. Mena, C.A. Ternes, M. Tórtola, J.W.F. Valle, 2020 global reassessment of the neutrino oscillation picture. JHEP **02**, 071 (2021)
69. S. Vagnozzi, E. Giusarma, O. Mena, K. Freese, M. Gerbino, S. Ho, M. Lattanzi, Unveiling ν secrets with cosmological data: neutrino masses and mass hierarchy. Phys. Rev. D **96**(12), 123503 (2017)
70. A. Boyarsky, M. Drewes, T. Lasserre, S. Mertens, O. Ruchayskiy, Sterile neutrino dark matter. Prog. Part. Nucl. Phys. **104**, 1–45 (2019)
71. S.R. Coleman, E.J. Weinberg, Radiative corrections as the origin of spontaneous symmetry breaking. Phys. Rev. D **7**, 1888–1910 (1973)
72. A. Mohamadnejad, Gravitational waves from scale-invariant vector dark matter model: probing below the neutrino-floor. Eur. Phys. J. C **80**(3), 197 (2020)
73. E. Gildener, S. Weinberg, Symmetry breaking and scalar bosons. Phys. Rev. D **13**, 3333 (1976)
74. S.J. Huber, T. Konstandin, Gravitational wave production by collisions: more bubbles. JCAP **09**, 022 (2008)
75. C. Caprini et al., Science with the space-based interferometer eLISA. II: Gravitational waves from cosmological phase transitions. JCAP **04**, 001 (2016)
76. M. Hindmarsh, S.J. Huber, K. Rummukainen, D.J. Weir, Shape of the acoustic gravitational wave power spectrum from a first order phase transition. Phys. Rev. D **96**(10), 103520 (2017) (**Erratum: Phys. Rev. D 101, 089902 (2020)**)

77. H.-K. Guo, K. Sinha, D. Vagie, G. White, Phase transitions in an expanding universe: stochastic gravitational waves in standard and non-standard histories. JCAP **01**, 001 (2021)
78. P. Binetruy, A. Bohe, C. Caprini, J.-F. Dufaux, Cosmological backgrounds of gravitational waves and eLISA/NGO: phase transitions. Cosmic strings and other sources. JCAP **06**, 027 (2012)
79. A. Vilenkin, Gravitational radiation from cosmic strings. Phys. Lett. B **107**, 47–50 (1981)
80. J.J. Blanco-Pillado, K.D. Olum, Stochastic gravitational wave background from smoothed cosmic string loops. Phys. Rev. D **96**(10), 104046 (2017)
81. D.I. Dunsky, A. Ghoshal, H. Murayama, Y. Sakakihara, G. White, GUTs, hybrid topological defects, and gravitational waves. Phys. Rev. D **106**(7), 075030 (2022)
82. J.J. Blanco-Pillado, K.D. Olum, B. Shlaer, The number of cosmic string loops. Phys. Rev. D **89**(2), 023512 (2014)
83. L. Sousa, P.P. Avelino, Stochastic gravitational wave background generated by cosmic string networks: velocity-dependent one-scale model versus scale-invariant evolution. Phys. Rev. D **88**(2), 023516 (2013)
84. Y. Cui, M. Lewicki, D.E. Morrissey, J.D. Wells, Probing the pre-BBN universe with gravitational waves from cosmic strings. JHEP **01**, 081 (2019)
85. Y. Gouttenoire, G. Servant, P. Simakachorn, Beyond the standard models with cosmic strings. JCAP **07**, 032 (2020)
86. S. Blasi, V. Brdar, K. Schmitz, Fingerprint of low-scale leptogenesis in the primordial gravitational-wave spectrum. Phys. Rev. Res. **2**(4), 043321 (2020)
87. P. Auclair et al., Probing the gravitational wave background from cosmic strings with LISA. JCAP **04**, 034 (2020)